4202–4211 *Nucleic Acids Research, 2005, Vol. 33, No. 13*
doi:10.1093/nar/gki688

The involvement of the aspartate triad of the active center in all catalytic activities of multisubunit RNA polymerase

Vasily Sosunov[1], Savva Zorov[2,3], Ekaterina Sosunova[1,4], Anatoly Nikolaev[1], Irina Zakeyeva[2], Irina Bass[4], Alex Goldfarb[1], Vadim Nikiforov[1,4], Konstantin Severinov[2,4,*] and Arkady Mustaev[1]

[1]Public Health Research Institute, 225 Warren Street, Newark, NJ 07103, USA, [2]Department of Molecular Biology and Biochemistry, Waksman Institute, Rutgers University, Piscataway, NJ 08854, USA, [3]A.N. Belozersky Institute, Moscow State University, Moscow, Russia and [4]Institute of Molecular Genetics, Russian Academy of Sciences, Moscow, Russia 123182

Received April 2, 2005; Revised June 6, 2005; Accepted June 14, 2005

ABSTRACT

Three conserved aspartate residues in the largest subunit of multisubunit RNA polymerases (RNAPs) coordinate two Mg^{2+} ions involved in the catalysis of phosphodiester bond synthesis. A structural model based on the stereochemistry of nucleotidyl transfer reaction as well as recent crystallographic data predict that these Mg^{2+} ions should also be involved in the reverse reaction of pyrophosphorolysis as well as in the endo- and exonucleolytic cleavage of the nascent RNA. Here, we check these predictions by constructing point substitutions of each of the three Asp residues in the β′ subunit of *Escherichia coli* RNAP and testing the mutant enzymes' functions. Using artificially assembled elongation complexes, we demonstrate that substitutions of any of the three aspartates dramatically reduce all known RNAP catalytic activities, supporting the model's predictions that same amino acids participate in all RNAP catalytic reactions. We demonstrate that though substitutions in the DFDGD motif decrease Mg^{2+} binding to free RNAP below detection limits, the apparent affinity to Mg^{2+} in transcription complexes formed by the mutant and wild-type RNAPs is similar, suggesting that NTP substrates and/or nucleic acids actively contribute to the retention of active center Mg^{2+}.

INTRODUCTION

A conserved triad of aspartic acid residues has been implicated in the catalytic mechanism of multisubunit cellular RNA polymerases (RNAPs) (1). The aspartates are contained in the invariant DFDGD motif in the largest RNAP subunit. Initially, the role of the triad in coordination of a catalytic Mg^{2+} ion was inferred from the properties of a triple alanine substitution mutant (2). RNAP harboring this mutation formed stable open promoter complexes but was catalytically inactive (2). In the crystal structure, the DFDGD motif is part of an apparently flexible loop that is attached to a rigid β-barrel domain (Figure 1A). The loop protrudes into the RNAP catalytic center and, in agreement with biochemical studies, chelates a divalent metal (Me^{2+}) ion (3,4). As expected, RNAP harboring the triple substitution failed to retain Me^{2+} ion in the catalytic center (2), thus providing an explanation for the lack of the catalytic activity.

In a previous communication, we used molecular modeling to propose a structural model of RNA polymerization reaction by multisubunit RNAPs (1). In the model, the three Asp residues from the DFDGD motif coordinate two Mg^{2+} ions (Figure 1B). Two of the carboxylates (Asp^{460} and Asp^{462} in *Escherichia coli* numbering) bridge both ions, while the third (Asp^{464}) interacts with only one of the ions, Mg^{2+} I. This ion is additionally coordinated by the 3′-hydroxyl on the RNA 3′-terminus and one of the oxygens of the NTP substrate's α-phosphate, which ensures an in-line attack of the 3′-hydroxyl group on the α-phosphorus atom. The second Mg^{2+} ion, Mg^{2+} II, contacts the three oxygen atoms of the

*To whom correspondence should be addressed. Tel: +1 732 445 6095; Fax: +1 732 445 5735; Email: severik@waksman.rutgers.edu
Correspondence may also be addressed to Arkady Mustaev. Tel: +7 973 854 3440; Fax: +7 973 854 3441; Email: arkady@phri.org

The authors wish to be known that, in their opinion, the first two authors should be regarded as joint First Authors

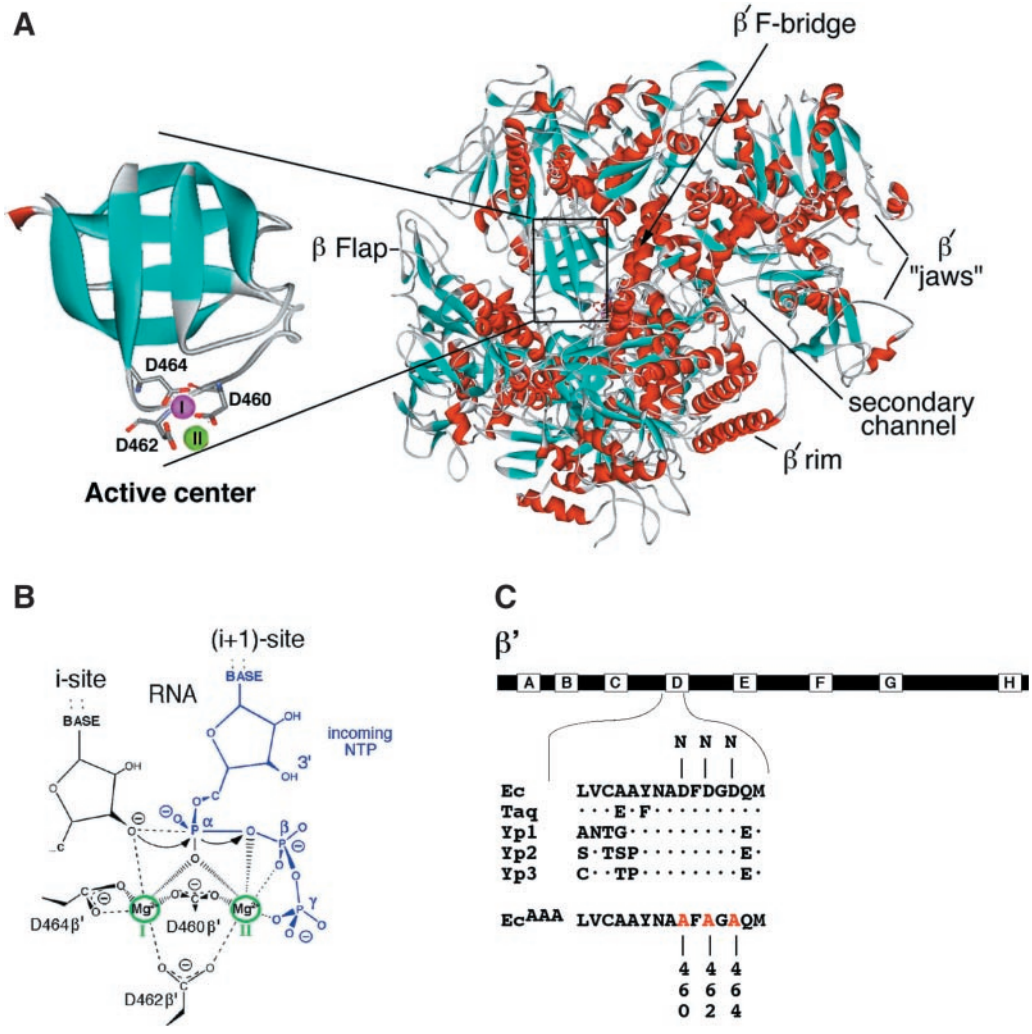

Figure 1. The catalytic center of multisubunit RNAP. (**A**) The structural context of RNAP active center. The structure of *Taq* RNAP core along with that of magnified domain of the active center is shown in ribbon representation. Color coding: α helixes—red, β strands—cyan, loops—gray, active center residues—element color. The main structural features of RNAP are indicated. Catalytic aspartates and Mg^{2+} ions are marked as in (B) (*E.coli* numbering). (**B**) The two Mg^{2+} ions (green) are coordinated by the three Asp residues (numbering for the *E.coli* RNAP β′ subunit). The NTP substrate is in blue. Arrows indicate the direction of electron density transfer during the polymerization reaction (1). (**C**) The bar schematically illustrates the 1407 amino acid long *E.coli* RNAP β′ subunit. The lettered boxes indicate evolutionarily conserved regions of the sequence. A fragment of evolutionarily conserved segment D primary sequence (in single-lettered code) is expanded underneath and is aligned with homologous sequences from *Thermus aquaticus* (*Taq*) and yeast RNAPs I, II and III (Yp1, Yp2 and Yp3, respectively). The three point substitutions analyzed in this work, D460N, D462N and D464N are shown above the *E.coli* sequence. The sequence of a triple alanine substitution studied previously (2) is shown below the alignment.

triphosphate chain of the substrate thus stabilizing the penta-coordinated intermediate and neutralizing the developing negative charge on the leaving pyrophosphate group. The predicted positions of the two Mg^{2+} ions and an NTP substrate were recently confirmed by high-resolution structural analysis of yeast RNAP II (5).

In the ternary elongation complex (TEC), multisubunit RNAP performs, in addition to the forward reaction of RNA polymerization, the reverse reaction of pyrophosphorolysis, the 3′–5′ hydrolysis of the nascent RNA, and the internal cleavage of RNA which is stimulated by specialized factors [called Gre factors in eubacteria, reviewed in (6)]. In our model, all of these activities are performed by the same active site and involve the same pair of Mg^{2+} ions (1). A similar proposal was made on the basis of crystallographic and biochemical analyses of bacterial RNAP complexes with Gre factor (7–9) and yeast RNAP II complexes with the SII nascent RNA cleavage factor (10,11). In this work, we set up to directly test the model's predictions by studying the effects of individual substitutions of Asp residues in the DFDGD motif in RNAP from *E.coli*. We find that in agreement with the model's predictions, substitutions of any of the three Asp residues dramatically decrease the rates of RNA polymerization, pyrophosphorolysis, and exo- and endonucleolytic cleavage reactions. We also find that though substitutions in the DFDGD motif decrease Mg^{2+} binding to free RNAP below detection limits, the apparent Mg^{2+} affinity of transcription complexes formed by the mutant and wild-type RNAPs is similar, suggesting that nucleic acids and/or NTP substrates actively contribute to the formation of the RNAP catalytic center.

MATERIALS AND METHODS

Engineering of *rpoC* mutations and preparation of recombinant RNAP

Mutations in *rpoC* codons 460, 462 and 464 were generated using PCR-mediated site-specific mutagenesis of the pET29β′ expression plasmid that harbors the wild-type *E.coli rpoC* fused to a 3′-terminal hexahistidine tag. Details of the mutagenesis strategy are available from the authors upon request. Mutations were verified by sequencing. Plasmids carrying mutant *rpoC* or control pET29β′ were transformed into BL21 (DE3) *E.coli* strain, and the β′ subunits were overproduced, purified and used for reconstitution of RNAP as described (12).

The previously described AAA RNAP triple mutant expression plasmid pMKA201 carrying the mutant gene was transformed in R120F- *lac his metB thi strA rpoC*ts [placIq(K)] *E.coli* which carries a temperature-sensitive mutation in the chromosomal copy of the *rpoC* (13). pMKA201 carrying the wild-type *rpoC* was used as a control. Cells were grown overnight in 4 l of LB media in presence of 200 μg/ml Ampicillin and 20 μg/ml Kanamycin at 30°C and harvested by centrifugation at 4°C. RNAP was purified exactly as described (14).

Artificially assembled transcriptional complexes and transcript elongation

The sequences of synthetic RNAs and DNA oligonucleotides used are shown in Figure 4A. RNA oligonucleotides were obtained from Oligos Etc., Inc. (Wilsonville, OR), DNA oligos were obtained from QIAGEN Operon (Valencia, CA). The sequence of DNA is based on that of T7 A1 promoter in the register −15 to +27 with regard to the start point of transcription. Prior to scaffold assembly, the RNA component was ^{32}P-labeled at the 5′ terminus using [γ-^{32}P]ATP and T4 polynucleotide kinase (New England Biolabs). To obtain TEC13, 1 pmol of RNAP core enzyme in 10 μl TB (transcription buffer, 40 mM Tris–HCl, pH 7.9, 100 mM KCl and 10 mM $MgCl_2$) was mixed with 4 μl of Ni-NTA agarose suspended in TB and incubated for 3 min at 25°C. One picomole (1 μl) of RNA/template DNA strand mix was added, incubated for 5 min at 37°C and washed (4 × 1 ml) with cold TB without $MgCl_2$ to avoid endonucleolytic cleavage. The pellet was resuspended in 15 μl TB without $MgCl_2$ followed by the non-template DNA (10 pmol) addition, incubated for 5 min at 37°C and washed with cold TB (4 × 1 ml). Transcription was initiated by the addition of all four NTPs (or CTP) and $MgCl_2$ (or $MnCl_2$). The times of the reaction and the concentrations of NTPs and $MgCl_2$ (or $MnCl_2$) are indicated in the figures or figure legends. For K_m measurements, reactions were performed under the conditions when no more than ∼25% of RNA was extended. The reactions were terminated by the addition of an equal volume of loading buffer containing 6 M urea, reaction products were resolved by denaturing PAGE and revealed by PhosphorImager (Molecular Dynamics).

Rapid elongation kinetics experiments

The experiments were performed with a KinTek Chemical Quench Flow Model RQF-3 mixer (KinTek Co., Austin, TX), which uses as little as 10 μl of sample per experiment and can measure reaction times as short as 5 ms. The settings and calibration of the Quench Flow device were accomplished according to the standard procedure suggested by the manufacturer. One of the two 10 μl sample loops was loaded with solution containing various concentrations of CTP and $MgCl_2$, the other loop was loaded with TEC13 complex prepared as described above. Prior to loading into the sample loop, transcription complexes were removed from Ni-NTA agarose by combining 5–10 μl of beads containing washed TEC13 with 12 μl of TB without $MgCl_2$ but with 200 mM imidazole, pH 7.9 and incubation for 1 min at room temperature. After brief centrifugation, transcription complexes were recovered in the supernatant. The reactants were mixed in the reaction loop, reaction was allowed to proceed for specified times and were stopped by 0.5 M EDTA which was supplied through a quench line (the final concentration of EDTA was ∼0.15 M). Control experiment, using a reverse reaction set up, where 0.5 M EDTA was provided through a sample loop and the CTP–$MgCl_2$ solution through a quench line showed that reactions were fully quenched in <5 ms. The reaction products were analyzed as above.

Endonuclease cleavage and pyrophosphorolysis

The endonucleolytic cleavage reactions were performed in the assembled TEC13 at 37°C in TB. GreA- and GreB-induced cleavage was performed using 20-fold molar excess of cleavage factors over RNAP. In the case of pyrophosphorolysis, 1 mM PPi was added to the TEC13. The reaction times varied from 2 to 15 min (for WT RNAP) and from 1 to 4 h (for mutant RNAPs). Reactions were stopped and products analyzed as described above.

Iron-mediated affinity cleavage

Fe^{2+}-mediated affinity cleavage was performed as in (2). RNAP (1 pmol) in 10 μl TB without $MgCl_2$ was combined with 10 mM DTT and $Fe(NH_4)_2(SO_4)_2$ in concentrations indicated in Figure 2, and incubated at 21°C for 20–70 min. The samples were supplemented with one-third (v/v) of 0.5 M Tris–HCl, pH 8.0, 5% DTT, 30% glycerol, 5% SDS and 0.05% Bromophenol blue, and the cleavage products were separated on a 8% SDS–polyacrylamide gel and stained with Coomassie R-250.

RESULTS

Substitutions of catalytic Asp residues abolish promoter-dependent transcription

To assess the role of individual Asp residues from the DFDGD motif, point mutations substituting Asp^{460}, Asp^{462} and Asp^{464} for Asn were engineered in the cloned *E.coli rpoC* gene coding for RNAP β′ (Figure 1C). The choice of substitutions was dictated by our desire to reduce the metal-binding ability while preserving the overall geometry of the residue. Mutant RNAPs were reconstituted from individually overexpressed subunits and purified using a published procedure (12). The mutant enzymes were completely inactive in the abortive initiation reaction as well as in the steady-state run-off RNA synthesis reaction from the T7 A1 promoter at conditions when the control wild-type (WT) enzyme was highly active

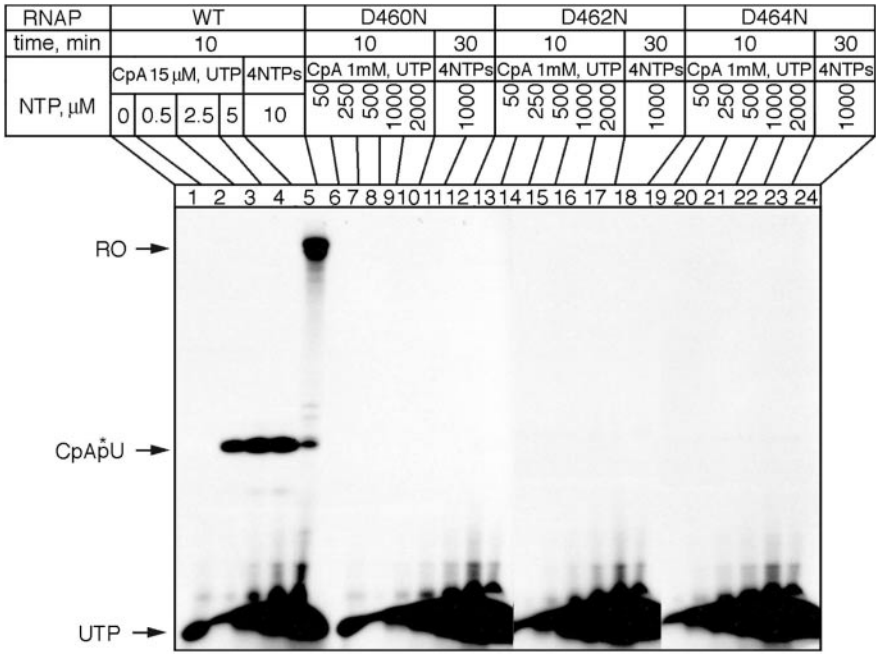

Figure 2. *In vitro* transcription by wild-type and mutant RNAPs. The indicated RNAPs were combined with a DNA fragment containing the T7 A1 promoter at conditions (i) supporting abortive synthesis of CpApU trinucleotide from the CpA primer and [α-^{32}P]UTP or (ii) supporting the steady-state synthesis of full-sized run-off (RO) product in the presence of all four NTPs. Reaction products were resolved by denaturing PAGE and revealed by autoradiography.

(Figure 2). Gel-retardation and $KMnO_4$ probing experiments revealed that the mutant enzymes were able to recognize, bind to, and open the T7 A1 promoter as efficiently as WT RNAP (data not shown). We conclude that each of the three Asp residues in the DFDGD motif is essential for promoter-dependent transcription by *E.coli* RNAP holoenzyme.

Substitutions of catalytic Asp residues interfere with Me^{2+} binding to free RNAP

To test the effect of individual Asp substitutions on divalent metal binding in the active center, we used Fe^{2+}-mediated cleavage assay. This assay utilizes the ability of Fe^{2+} ions chelated in the active center instead of Mg^{2+} to cleave nearby sites in the protein through generation of hydroxyl radicals (2). Incubation of the WT RNAP in the presence of 20 μM Fe^{2+} caused the appearance of ~115 and 45 kDa polypeptides (Figure 3, lanes 2 and 3), which are the products of the β′ subunit cleavage at the DFDGD motif (2). As expected, the cleavage occurred only in the presence of DTT (Figure 3, lane 3), i.e. it was dependent on hydroxyl radicals. No cleavage products were detected when the mutant enzymes were subjected to Fe^{2+}-mediated cleavage even in the presence of 70 μM Fe^{2+} (Figure 3, lanes 6, 9 and 12). We therefore conclude that substitution of either one of the three Asp residues in the DFDGD motif interferes with Me^{2+} binding to free RNAP. Thus, RNAP carrying single amino acid substitutions in the DFDGD motif behave similarly to the previously described RNAP harboring a triple Asp–Ala substitution in the motif (2).

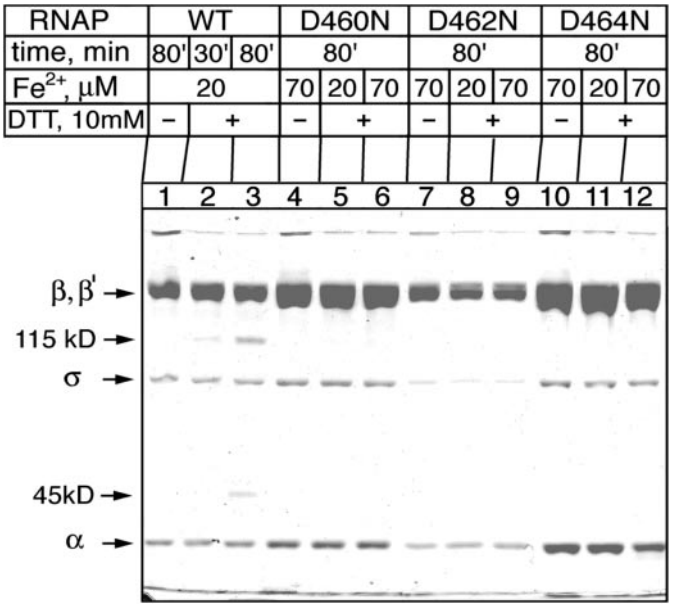

Figure 3. Fe^{2+}-mediated affinity cleavage of wild-type and mutant RNAPs. RNAPs were subjected to Fe^{2+}-mediated affinity cleavage in the presence of various concentrations of Fe^{2+} for the times indicated. Reaction products were resolved by SDS–PAGE and revealed by Coomassie blue staining. The positions of intact RNAP subunits and of main products of Fe^{2+}-mediated cleavage of the β′ subunit (115 and 45 kDa) are indicated.

Mutant RNAPs are partially active on nucleic acid scaffolds

The inability of mutant RNAPs to synthesize RNA in a standard promoter-dependent assay made it impossible to test their RNA degradation activities. To overcome this problem, we used artificial elongation complexes assembled on a synthetic nucleic acid scaffold that mimics the architecture of nucleic acids in a natural transcription elongation complex (15,16). The scaffold system allows to study reactions

characteristic of TEC directly, bypassing complex reactions involved in *de novo* initiation of RNA chains.

The DNA component of the scaffold used in our experiments was based on the T7 A1 promoter sequence (positions −15 to +27) with several substitutions introduced to avoid hairpin formation (Figure 4A). The RNA component of the scaffold corresponded to the 13 nt long T7 A1 promoter transcript. We chose this particular scaffold because the corresponding natural TEC is particularly prone to reactions of internal cleavage and pyrophosphorolysis (our unpublished observations).

WT RNAP complexed with nucleic acid scaffold exhibited catalytic activities typical of natural TEC (Figure 4B). As can be seen, the initial RNA product, 13A (lane 1), was extended to 14C in the presence of CTP (lane 3) and to longer products in the presence of four NTPs (lane 4). The addition of pyrophosphate-induced processive degradation of the 13A RNA (lane 5). Incubation in the absence of NTPs led to shortening of the 13A RNA to 11A due to intrinsic endonucleolytic cleavage activity of the RNAP catalytic center (lane 2); this activity was further stimulated by transcript cleavage factors GreA and GreB (lanes 6 and 7). It should be noted that factor-dependent cleavage in scaffold complexes required stoichiometric amounts of cleavage factors. This is in contrast to the situation described for natural elongation complexes, where Gre factors act catalytically (17). The reason for this difference is currently unknown; stronger binding of Gre factors to artificially assembled TECs or lesser tendency of artificially assembled TECs to backtrack may be responsible, though this was not further investigated.

All three Asp/Asn substitution mutants were tested for their ability to extend the 13A RNA in the scaffold complex and the results are presented in Figure 4C. As can be seen, all three mutants displayed noticeable levels of RNA polymerization activity in this system. The D462N mutant appeared to be the most active (lanes 11–16). The RNA polymerization activity of the mutant enzymes increased at elevated concentrations of NTPs and at higher temperatures (compare, e.g. lanes 13 and 15, and lanes 15 and 16, respectively). However, the mutants were clearly much less active than WT RNAP: while the WT enzyme completed the elongation of the 13A RNA into a run-off product after a 5 min incubation with 1 mM NTPs (lane 3), none of the mutants did even after a 15 min incubation (lanes 9, 15 and 21, for D46N, D462N and D464N, respectively). The RNA polymerization activity in reactions containing RNAP mutants could not be due to the presence of contaminating WT RNAP, since the contaminating enzyme would have completely elongated the 13A transcript. Therefore, we conclude that the mutant enzymes can elongate the RNA primer in nucleic acid scaffolds. Compared to the WT RNAP, the mutant enzymes are severely defective and the nascent RNA elongation is very slow.

The activity of the previously described triple Asp–Ala substitution mutant (Figure 1C) was also tested using nucleic acid scaffolds. Unlike the single-substitution mutants, the triple mutant was completely inactive in the nascent transcript elongation even when reaction was allowed to proceed for several hours (Figure 4D, lane 8).

No conclusions about the nature of the strong defect exhibited by the single-substitution mutants in the forward reaction

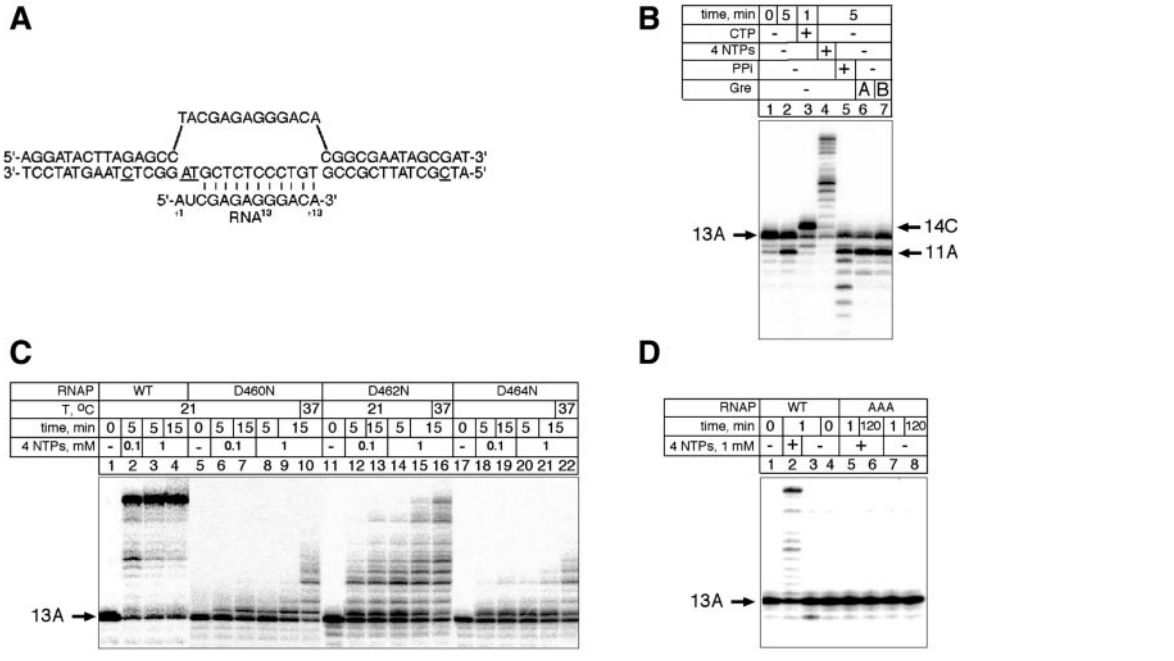

Figure 4. Activity of WT and mutant RNAPs in artificially assembled nucleic acid scaffold complexes. (**A**) The structure of the 13A scaffold. Base pairing in the RNA/DNA hybrid is shown. (**B**) The 13A scaffold with 5′-terminally ^{32}P-labeled RNA component was combined with wild-type RNAP. The complex was subjected to the indicated treatments and reaction products were separated by denaturing PAGE and revealed by autoradiography. Reaction products are identified by their size (numbers) and the nature of the 3′-terminal nucleotide (letters). (**C**) 13A scaffold complexes were assembled using WT RNAP or RNAP mutants carrying single Asp–Asn substitutions and incubated in the presence of indicated concentrations of NTPs for various times. Reaction products were analyzed as in B. (**D**) As in C, except that a triple Asp–Ala mutant was used for scaffold complex assembly.

of RNA synthesis (i.e. whether substitutions affect NTP binding or the rate of catalysis) can be made from the experiment presented in Figure 4C, since the wild-type enzyme completes the reaction during the time of the experiment (in fact, at 37°C and in the presence of 1 mM NTPs, a condition when the mutant enzymes incompletely elongated the 13A RNA even after a 15 min incubation, the wild-type enzyme completed the reaction in several seconds, data not shown). Moreover, elongation of the 13A RNA by the mutants resulted in the appearance of multiple extension products, making quantification of the results difficult. To overcome these problems, we studied elongation of the 13A RNA in the presence of CTP, which allows only a single step of nucleotide addition reaction to occur. The slow single nucleotide addition reaction by the mutant enzymes was studied using manual sampling; the fast reaction by the wild-type RNAP was studied using a quench flow device.

To determine the reaction rates and apparent K_m values (with respect to the CTP substrate), the conversion of 13A to 14C was studied as a function of time and of the CTP concentration (the latter varied from 1 μM to 2 mM). For a given concentration of CTP, the reaction rates were determined from linear portions of time-dependence curves at conditions when <30% of the initial RNA was extended. The apparent rate constants were calculated from the equation $k_{app} = v_0/[S_0]$ (where v_0 is initial extension rate and $[S_0]$—initial concentration of TEC) and plotted as a function of [CTP]. From the resulting hyperbolic curve, V_{max} was determined as the reaction rate at saturating concentration of CTP. K_m was calculated as the concentration of NTP at which the reaction rate was half of the maximal. The observed rates for the three mutants at saturating (2 mM) CTP concentration are presented in Table 1. As can be seen, substitutions in the DFDGD motif led to dramatic decrease in the rate of nucleotide addition. Substitutions in the DFDGD motif did not significantly alter the apparent K_m values which ranged from 25 μM (D460N) to 200 μM (D464N), with the WT RNAP showing an intermediate value (100 μM). It is clear that these small differences cannot account for dramatic differences in reaction rates between the wild-type and the mutant enzymes.

Table 1. Rate constants and relative rates of reactions catalyzed by WT and mutant RNAPs

	$RNAP^{WT}$	$RNAP^{D460N}$	$RNAP^{D462N}$	$RNAP^{D464N}$
Elongation				
2 mM CTP, 10 mM Mg^{2+}	3500	0.06	1.4	0.7
WT/mutant		58 000	2500	5000
Mn^{2+}/Mg^{2+}[a]	1.25	75	20	50
Pyrophosphorolysis				
1 mM PPi, 10 mM Mg^{2+}	0.8	7×10^{-4}	8×10^{-4}	10^{-4}
WT/mutant		1100	1000	8000
Intrinsic cleavage				
10 mM Mg^{2+}	0.14	7×10^{-4}	2×10^{-4}	10^{-4}[b]
WT/mutant		200	700	1400
Mn^{2+}/Mg^{2+}	12	6	6	<3
GreA cleavage	0.93	2×10^{-3}	2×10^{-4}	3.7×10^{-3}
WT/mutant		460	4600	250
GreA/intrinsic cleavage	6.6	2.9	1	37
GreB cleavage	0.6	10^{-3}	0.2×10^{-3}	0.2×10^{-3}
WT/mutant		600	3000	3000
GreB/intrinsic cleavage	4.3	1.4	1	2

The data presented are calculated k_{obs} (min^{-1}). Rates of RNA elongation were measured at 21°C. Rates of RNA cleavage were measured at 37°C.
[a]Measured at 1 μM of CTP.
[b]Detection limit in this assay is determined by the fact that incubations longer than 30 min result in appearance of non-enzymatic RNA degradation products.

Asp substitutions only moderately reduce apparent affinity of the catalytic center to Me^{2+} in transcription complexes

It is tempting to speculate that strong catalytic defects exhibited by the mutant enzymes are due to their inability to bind the catalytic Mg^{2+}. To test this idea, we determined the effect of various Mg^{2+} concentrations on the single-step extension reaction of 13A RNA. The experiment was performed at low concentration of CTP to prevent the drop in concentration of free Mg^{2+} due to chelation by NTP. The apparent Mg^{2+} binding constants calculated from these data were 0.2, 0.4, 0.6 and 0.8 mM for WT, D460, D462 and D464, correspondingly (Figure 5). The result suggests that in nucleic acid scaffold complexes, Asp–Asn substitutions lead to a small (<5-fold) effect on Mg^{2+} binding. Moreover, since our standard reaction buffer contains high (10 mM) concentration of Mg^{2+}, the very large catalytic defect exhibited by the mutant enzymes could not be caused by decreased Mg^{2+} binding.

Mutational analysis of active center mutants in DNA polymerases showed that some mutants can be rescued by substituting Mg^{2+} ion in the reaction buffer for Mn^{2+} (18–20), apparently because the larger Mn^{2+} ion is better retained or because its orientation is more restricted in the mutant active center. Mn^{2+} can substitute for Mg^{2+} in transcription (21). We therefore tested the effect of Mn^{2+} on the conversion of 13A to 14C complex. Substitution of Mg^{2+} for Mn^{2+} had little effect on WT RNAP but strongly stimulated the mutant enzymes (Table 1). However, even in the presence of saturating concentrations of Mn^{2+}, the catalytic activity of mutant RNAPs was dramatically diminished compared to WT RNAP activity. We therefore conclude that saturating concentrations of either

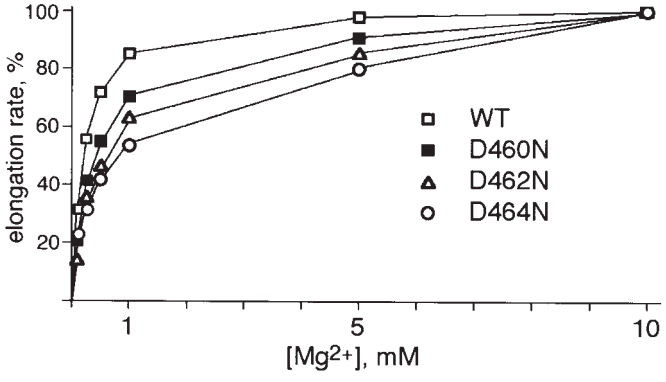

Figure 5. Residual activity of mutant RNAP at different concentration of Mg^{2+}. Single nucleotide addition reaction (Figure 4B, lane 2) was performed in the presence of 1 μM CTP and indicated concentrations of Mg^{2+}. For each enzyme, the extent of 13A RNA elongation in the presence of 10 mM Mg^{2+} was taken to be 100%. Each value represents a mean of three independent measurements.

Mg^{2+} or Mn^{2+} ions are unable to rescue the mutant enzymes' activity.

Transcript cleavage by mutant RNAPs

Since mutant enzymes form active complexes with the nucleic acid scaffold, we tested the effect of Asp substitutions on the rate of pyrophosphorolysis (quantified from the rate of accumulation of multiple products of pyrophosphorolysis, see Figure 4B, lane 5), intrinsic RNA cleavage (quantified from the rate of accumulation of band 11A, see Figure 4B, lane 2) and Gre factor-dependent cleavage (quantified from the rate of accumulation of band 11A, Figure 4B, lanes 6 and 7). Since the cleavage reactions performed by the WT enzyme are relatively slow, characteristic rate constants could be determined from time course experiments with manual sampling. The results, which are summarized in Table 1, show that RNA degradation was dramatically reduced by all three substitutions. However, each substitution led to a characteristic pattern of residual degradation activity. For example, substitution of Asp^{464} reduced intrinsic cleavage below the sensitivity of the assay, while substitutions of Asp^{460} and Asp^{462} resulted in detectable levels of cleavage. Curiously, though Mn^{2+} stimulated the forward (RNA elongation) reaction of the mutant enzymes more than the WT enzyme reaction, the reverse was true for the intrinsic cleavage reaction, where, relative to WT RNAP, the defect of the mutant enzymes increased in the presence of Mn^{2+} (Table 1). With respect to Gre factor-dependent cleavage of the nascent RNA, only the Asp^{464} mutant, which had undetectable intrinsic cleavage activity, was stimulated by GreA (Table 1). However, even in the presence of the factor, the transcript cleavage rate still remained slow compared to that seen with WT RNAP. From these data, we conclude that substitutions in the DFDGD motif affect not only the reaction of RNA synthesis, but also the reverse reaction of pyrophosphorolysis and the intrinsic endonucleolytic cleavage reaction. The result thus agrees with a model that posits that all of the known catalytic activities of RNAP are due to Mg^{2+} ions bound in a single catalytic center (1).

DISCUSSION

The principal observation of this work is that each of the three Asp/Asn substitutions in the RNAP metal-binding center causes dramatic reduction of all RNAP catalytic activities (summarized in Table 1). For each mutant RNAP, the drop in catalytic activity was comparable to that seen in single subunit polymerases—such as DNA polymerase (DNAP) I, DNAP β, HIV reverse transcriptase etc.—carrying substitutions of catalytic residues (18,20,22–27). From this, we conclude that in multisubunit RNAPs, each member of the Asp triad directly participates in the catalytic function.

Each of the substitutions caused a strong reduction in retention of the tightly bound Me^{2+} in free RNAP, as is evident from the failure of the mutants to support Fe^{2+}-mediated protein cleavage and from the failure of elevated concentrations of Fe^{2+} to compensate for the defect. The result is in agreement with a model where in the free enzyme, each of the three aspartates directly coordinates Mg^{2+} I (Figure 1B). Based on the sensitivity of Coomassie stain used to reveal Fe^{2+} cleavage products, we estimate that in free RNAP, individual substitutions decrease the affinity to Fe^{2+} by at least 20-fold. This is in good agreement with a ~30-fold effect expected from a loss of one coordinating bond as follows from comparisons of Mg^{2+} dissociation constants of citrate (Cit^{3-}) and oxalate (Ox^{2-}) ions [10^{-4} and 3×10^{-3} M respectively, (28)]. Interestingly, the former value is close to the previously determined Mg^{2+} dissociation constant for free WT RNAP (29).

In TEC, the apparent loss of affinity to Mg^{2+} caused by Asp–Asn substitutions was <10-fold. This may indicate that interactions made by Mg^{2+} in free RNAP and in TEC are not equivalent. Evidently, the phosphates of incoming NTP and/or the 3′-hydroxyl of RNA contribute to Mg^{2+} binding in TEC and compensate for the defect seen in free RNAP (Figure 1B). In addition, the general decrease in free energy of the assembled active center may also have a stabilizing effect.

Clearly, the observed decreases in affinity to Me^{2+} ions in the mutants cannot quantitatively account for the observed dramatic drop in catalytic activity (Table 1). Indeed, elevated concentrations of Me^{2+} did not rescue the catalytic function of the mutants. In other words, even when Me^{2+} saturated the mutant enzyme, its catalytic center continued to malfunction. Each of the substitutions caused only slight changes in the apparent K_m for incoming CTP substrate that cannot account for the observed drop in catalytic activity. These observations indicate that the substitutions studied here must affect the chemistry of phosphodiester bond formation, most probably by altering the orientation of catalytic Mg^{2+} ions in the active center. Mechanistic interpretation of variations in catalytic activities exhibited by the mutants lies beyond the resolution of our present genetic and biochemical analyses and will have to await the results of structural analysis.

In a previous work (1), we proposed a unified model of multisubunit RNAP activities whereby all reactions of degradation and synthesis observed in TEC are carried out with the use of the same two Mg^{2+} ions coordinated by the same Asp triad. In agreement with the model, pyrophosphorolysis, which is a true reversal of polymerization, was dramatically slowed down as a result of point substitutions in the DFDGD motif studied here. More significantly, the substitutions also reduced the internal cleavage of RNA in TEC. This strongly favors the notion that the endonuclease reaction is mechanistically related to polymerization and pyrophosphorolysis and is assisted by the same Asp residues of the active center. The strong inhibitory effect of Asp substitutions on GreA, GreB-assisted RNA cleavage was also observed, in accordance with the view (1) that the Gre proteins merely stimulate the enzyme's active center by donating additional carboxylate residues for coordination of weakly bound Me^{2+} II.

Recent determination of the structure of yeast RNAP II elongation complex with bound nucleotide substrate (5) confirmed the general orientation of the NTP and the position of the catalytic Mg^{2+} ions in the active center inferred from our modeling (1). In Figure 6A, we aligned the active site from yeast TEC structure with active sites of single subunit polymerases in such a way that the position of the substrate's triphosphate and of the two coordinated Me^{2+} ions coincided to the maximum extent. As can be seen, the three Asp residues of the multisubunit RNAP have their counterparts in the

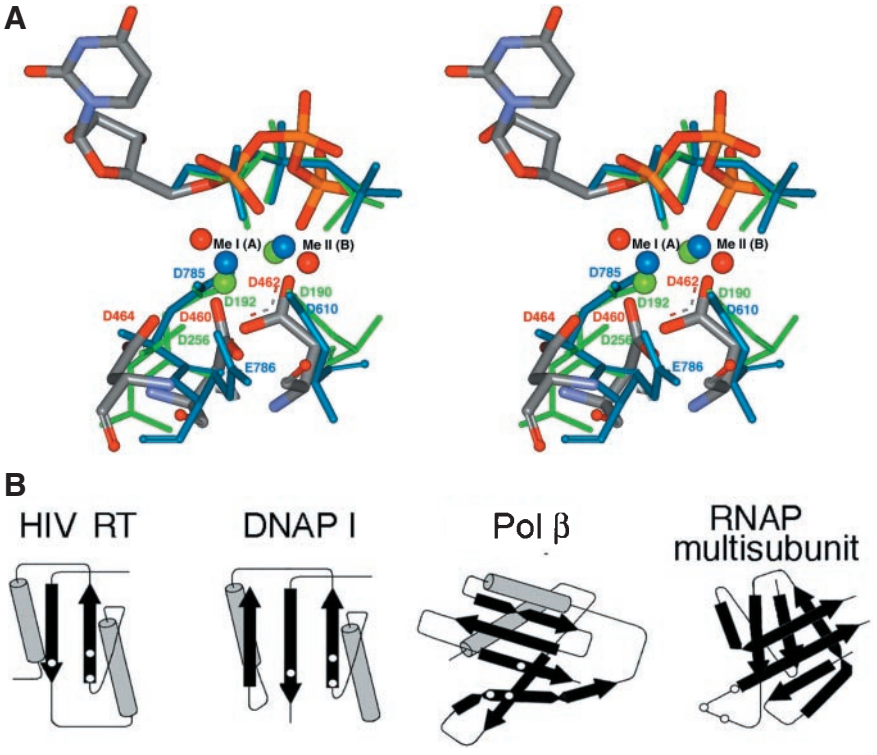

Figure 6. Comparative architecture of NTP polymerases' active centers. (**A**) Stereo view (for crossed eyes) of structural alignment of the catalytic carboxylate residues, the metal ions and the triphosphate chain of the NTP substrate for *Taq* DNAP I (light blue) (35), DNAP β (green) (32) and yeast RNAP II (element colors, the numbering is for *E.coli* β′) (5). For RNAP, the nucleoside part of the NTP substrate is shown. The carboxylate residues are marked, the Me^{2+} ions—numbered. (**B**) The architecture of active center domains for NTP polymerases. β strands and α helixes are shown as ribbons and barrels, respectively. The catalytic acidic residues are represented by white circles. For all enzymes, the view is from the same angle after aligning of the triphosphate chains of the NTP substrate in the co-crystal structure of the enzyme–substrate complex.

smaller enzymes. In each case, a bridging pair of residues (corresponding to Asp^{460} and Asp^{462} in *E.coli* RNAP β′) could be identified. These are Asp^{610} and Asp^{785} in DNAP I, Asp^{192} and Asp^{190} in DNAP β, and Asp^{110} and Asp^{185} in HIV reverse transcriptase (not shown). The analog of non-bridging Asp (Asp^{464} in *E.coli*) was also found in all cases with the exception of T7 RNAP (not shown).

While the general spatial orientation of the Asp triad residues is analogous in all types of polymerases, there is considerable difference in the arrangement of specific Asp residues in different enzymes. An example is the non-alignment of the bridging residue Asp^{482} in yeast RNAP II (Asp^{460} in *E.coli* RNAP) and equivalent Asp^{256} in DNAP β and Asp^{785} in DNAP I. In RNAP, this residue is shifted down ∼2 Å and rotated ∼90° relative to DNAP residues. Another example is the oxygen of the NTP β phosphate, which in yeast RNAP II is too faraway (∼4 Å) from Me^{2+} II for coordination.

While in single subunit polymerases, the orientation of the catalytic components is nearly perfect with respect to proposed catalytic mechanism (30), significant deviations from catalytically competent arrangement of the substrate, catalytic carboxylate residues, and of Me^{2+} II are observed in yeast RNAP II. However, the coordination geometry in the transition state should be similar in all cases since the catalytic mechanism for all polymerases is the same (30). This apparent inconsistency may be explained by specific architecture of the active center of cellular RNAP. As is schematically shown on Figure 6B, the general protein architecture that buttresses acidic residues chelating catalytic Mg^{2+} ions in multisubunit RNAPs is different from that found in single subunit polymerases. In single subunit enzymes, the catalytic aspartates are located in distant sites of the linear sequence and are brought together on anti-parallel β-structures supported by an α-helical base. As a result, the active site residues project from rigid scaffolds and require minimal structural adjustment for proper coordination of catalytic Me^{2+} and for substrate binding. In multisubunit RNAPs, the compact Asp triad resides in an apparently flexible loop flanked by a set of β-strands assembled in a barrel-like structure. As a result, in multisubunit RNAP the catalytic carboxylates are more flexible. In fact, the structure of the yeast RNAP II TEC with bound NTP may represent an inactive intermediate on its way to true ground state. This conjecture is supported by modeling that shows that an orientation of the NTP substrate, catalytic Asp residues, and Me^{2+} ions that is nearly identical to that found in single subunit polymerases can be obtained by moderate reshaping of the catalytic loop carrying the DFDGD motif (data not shown).

Flexible active center can also explain substrate selection by multisubunit RNAP. Biochemical evidence suggests that conserved Asn^{458} just upstream of the DFDGD motif contributes to discrimination between ribo- and deoxy-NTPs (31). However, in the structure of yeast RNAP II the corresponding residue is too far away (5 Å) from the 2′-hydroxyl of the bound

substrate. The reshaping of the catalytic loop mentioned above brings the side chain of Asn^{458} close enough to the 2′-hydroxyl to allow recognition through hydrogen-bonding (data not shown). Thus, binding of the 'proper' ribo-NTP can also simultaneously tune the active center for catalysis.

The tuning of active center in multisubunit RNAP can explain another fundamental difference between the two classes of polymerases related to RNA degradation reactions. Though both nucleic acid synthesis and degradation occur through the same chemical mechanism (30), different optimal conformations are probably required for each reaction. Our results show that the tunable active center in multisubunit RNAPs is flexible enough to perform polymerization, pyrophosphorolysis, 3′–5′ hydrolysis and the internal cleavage of RNA stimulated by the Gre proteins. The fact that individual substitutions in the DFDGD motif affect polymerization and degradation activities by RNAP to different extent suggest that different substitutions have differential effects on the ability of RNAP active site to adopt optimal conformations for these reactions. The fact that in DNAPs, the polymerase and nuclease activities are performed by different active sites may be due to inflexibility of the 'primary' polymerizing site.

In contrast to small polymerases, multisubunit RNAPs are highly regulated. Previous studies (32–34) suggested that regulatory signals such as specific nucleic acid sequences or protein factors can alter the catalytic activity of the RNAP. It is tempting to speculate that some of these signals might exert their effect by changing the conformation of the active center loop.

ACKNOWLEDGEMENTS

We thank Michael Kashlev for providing us with a plasmid carrying a triple mutation in the DFDGD motif and Sergei Nechaev for careful reading of the manuscript. This work was supported by NIH grant GM30717 to A.G., NIH grant GM64503 and Charles and Johanna Busch research grant to K.S., and by the Russian Foundation for Basic grant 02-04-48525. Funding to pay the Open Access publication charges for this article was provided by NIH GM30717.

Conflict of interest statement. None declared.

REFERENCES

1. Sosunov,V., Sosunova,E., Mustaev,A., Bass,I., Nikiforov,V. and Goldfarb,A. (2003) Unified two-metal mechanism of RNA synthesis and degradation by RNA polymerase. *EMBO J.*, **22**, 2234–2244.
2. Zaychikov,E., Martin,E., Denissova,L., Kozlov,M., Markovtsov,V., Kashlev,M., Heumann,H., Nikiforov,V., Goldfarb,A. and Mustaev,A. (1996) Mapping of catalytic residues in the RNA polymerase active center. *Science*, **273**, 107–109.
3. Zhang,G., Campbell,E.A., Minakhin,L., Richter,C., Severinov,K. and Darst,S.A. (1999) Crystal structure of *Thermus aquaticus* core RNA polymerase at 3.3 A resolution. *Cell*, **98**, 811–824.
4. Gnatt,A.L., Cramer,P., Fu,J., Bushnell,D.A. and Kornberg,R.D. (2001) Structural basis of transcription: an RNA polymerase II elongation complex at 3.3 A resolution. *Science*, **292**, 1876–1882.
5. Westover,K.D., Bushnell,D.A. and Kornberg,R.D. (2004) Structural basis of transcription: nucleotide selection by rotation in the RNA polymerase II active center. *Cell*, **119**, 481–489.
6. Borukhov,S., Laptenko,O. and Lee,J. (2001) *Escherichia coli* transcript cleavage factors GreA and GreB: functions and mechanisms of action. *Methods Enzymol.*, **342**, 64–76.
7. Opalka,N., Chlenov,M., Chacon,P., Rice,W.J., Wriggers,W. and Darst,S.A. (2003) Structure and function of the transcription elongation factor GreB bound to bacterial RNA polymerase. *Cell*, **114**, 335–345.
8. Sosunova,E., Sosunov,V., Kozlov,M., Nikiforov,V., Goldfarb,A. and Mustaev,A. (2003) Donation of catalytic residues to RNA polymerase active center by transcription factor Gre. *Proc. Natl Acad. Sci. USA*, **100**, 15469–15474.
9. Laptenko,O., Lee,J., Lomakin,I. and Borukhov,S. (2003) Transcript cleavage factors GreA and GreB act as transient catalytic components of RNA polymerase. *EMBO J.*, **22**, 6322–6334.
10. Kettenberger,H., Armache,K.J. and Cramer,P. (2004) Complete RNA polymerase II elongation complex structure and its interactions with NTP and TFIIS. *Mol Cell*, **16**, 955–965.
11. Kettenberger,H., Armache,K.J. and Cramer,P. (2003) Architecture of the RNA polymerase II–TFIIS complex and implications for mRNA cleavage. *Cell*, **114**, 347–357.
12. Borukhov,S. and Goldfarb,A. (1993) Recombinant *Escherichia coli* RNA polymerase: purification of individually overexpressed subunits and *in vitro* assembly. *Protein Expr. Purif.*, **4**, 503–511.
13. Nedea,E.C., Markov,D., Naryshkina,T. and Severinov,K. (1999) Localization of *Escherichia coli* rpoC mutations that affect RNA polymerase assembly and activity at high temperature. *J. Bacteriol.*, **181**, 2663–2665.
14. Kashlev,M., Nudler,E., Severinov,K., Borukhov,S., Komissarova,N. and Goldfarb,A. (1996) Histidine-tagged RNA polymerase of *Escherichia coli* and transcription in solid phase. *Methods Enzymol.*, **274**, 326–334.
15. Sidorenkov,I., Komissarova,N. and Kashlev,M. (1998) Crucial role of the RNA:DNA hybrid in the processivity of transcription. *Mol. Cell*, **2**, 55–64.
16. Korzheva,N., Mustaev,A., Nudler,E., Nikiforov,V. and Goldfarb,A. (1998) Mechanistic model of the elongation complex of *Escherichia coli* RNA polymerase. *Cold Spring Harb. Symp. Quant. Biol.*, **63**, 337–345.
17. Borukhov,S., Sagitov,V. and Goldfarb,A. (1993) Transcript cleavage factors from *E.coli*. *Cell*, **72**, 459–466.
18. Copeland,W.C. and Wang,T.S. (1993) Mutational analysis of the human DNA polymerase alpha. The most conserved region in alpha-like DNA polymerases is involved in metal-specific catalysis. *J. Biol. Chem.*, **268**, 11028–11040.
19. Saturno,J., Lazaro,J.M., Blanco,L. and Salas,M. (1998) Role of the first aspartate residue of the 'YxDTDS' motif of phi29 DNA polymerase as a metal ligand during both TP-primed and DNA-primed DNA synthesis. *J. Mol. Biol.*, **283**, 633–642.
20. Pritchard,A.E. and McHenry,C.S. (1999) Identification of the acidic residues in the active site of DNA polymerase III. *J. Mol. Biol.*, **285**, 1067–1080.
21. Rhodes,G. and Chamberlin,M.J. (1974) Ribonucleic acid chain elongation by *Escherichia coli* ribonucleic acid polymerase. I. Isolation of ternary complexes and the kinetics of elongation. *J. Biol. Chem.*, **249**, 6675–6683.
22. Bonner,G., Patra,D., Lafer,E.M. and Sousa,R. (1992) Mutations in T7 RNA polymerase that support the proposal for a common polymerase active site structure. *EMBO J.*, **11**, 3767–3775.
23. Zakharova,E., Wang,J. and Konigsberg,W. (2004) The activity of selected RB69 DNA polymerase mutants can be restored by manganese ions: the existence of alternative metal ion ligands used during the polymerization cycle. *Biochemistry*, **43**, 6587–6589.
24. Date,T., Yamamoto,S., Tanihara,K., Nishimoto,Y. and Matsukage,A. (1991) Aspartic acid residues at positions 190 and 192 of rat DNA polymerase beta are involved in primer binding. *Biochemistry*, **30**, 5286–5292.
25. Menge,K.L., Hostomsky,Z., Nodes,B.R., Hudson,G.O., Rahmati,S., Moomaw,E.W., Almassy,R.J. and Hostomska,Z. (1995) Structure–function analysis of the mammalian DNA polymerase beta active site: role of aspartic acid 256, arginine 254, and arginine 258 in nucleotidyl transfer. *Biochemistry*, **34**, 15934–15942.
26. Kaushik,N., Rege,N., Yadav,P.N., Sarafianos,S.G., Modak,M.J. and Pandey,V.N. (1996) Biochemical analysis of catalytically crucial aspartate mutants of human immunodeficiency virus type 1 reverse transcriptase. *Biochemistry*, **35**, 11536–11546.

27. Li,Y., Korolev,S. and Waksman,G. (1998) Crystal structures of open and closed forms of binary and ternary complexes of the large fragment of *Thermus aquaticus* DNA polymerase I: structural basis for nucleotide incorporation. *EMBO J.*, **17**, 7514–7525.
28. Lur'e,Yu. (1989) *Handbook on Analytical Chemistry*Khimia, Moscow.
29. Mustaev,A., Kozlov,M., Markovtsov,V., Zaychikov,E., Denissova,L. and Goldfarb,A. (1997) Modular organization of the catalytic center of RNA polymerase. *Proc. Natl Acad. Sci. USA*, **94**, 6641–6645.
30. Steitz,T.A. (1999) DNA polymerases: structural diversity and common mechanisms. *J. Biol. Chem.*, **274**, 17395–17398.
31. Svetlov,V., Vassylyev,D.G. and Artsimovitch,I. (2004) Discrimination against deoxyribonucleotide substrates by bacterial RNA polymerase. *J. Biol. Chem.*, **279**, 38087–38090.
32. Pelletier,H., Sawaya,M.R., Wolfle,W., Wilson,S.H. and Kraut,J. (1996) Crystal structures of human DNA polymerase beta complexed with DNA: implications for catalytic mechanism, processivity, and fidelity. *Biochemistry*, **35**, 12742–12761.
33. Epshtein,V., Mustaev,A., Markovtsov,V., Bereshchenko,O., Nikiforov,V. and Goldfarb,A. (2002) Swing-gate model of nucleotide entry into the RNA polymerase active center. *Mol. Cell*, **10**, 623–634.
34. Toulokhonov,I., Artsimovitch,I. and Landick,R. (2001) Allosteric control of RNA polymerase by a site that contacts nascent RNA hairpins. *Science*, **292**, 730–733.
35. Polesky,A.H., Dahlberg,M.E., Benkovic,S.J., Grindley,N.D. and Joyce,C.M. (1992) Side chains involved in catalysis of the polymerase reaction of DNA polymerase I from *Escherichia coli*. *J. Biol. Chem.*, **267**, 8417–8428.